Drying of an aerogel-based coating system in Swedish climates: Field tests and simulations

Downloaded from: https://research.chalmers.se, 2025-12-04 22:36 UTC

Citation for the original published paper (version of record):
Karim, A., Sasic Kalagasidis, A., Johansson, P. (2024). Drying of an aerogel-based coating system in Swedish climates: Field tests and simulations. Journal of Building Engineering, 84.
http://dx.doi.org/10.1016/j.jobe.2024.108532

N.B. When citing this work, cite the original published paper.

research.chalmers.se offers the possibility of retrieving research publications produced at Chalmers University of Technology. It covers all kind of research output: articles, dissertations, conference papers, reports etc. since 2004. research.chalmers.se is administrated and maintained by Chalmers Library

(article starts on next page)

Journal of Building Engineering 84 (2024) 108532

Contents lists available at ScienceDirect

Journal of Building Engineering

journal homepage: www.elsevier.com/locate/jobe

Drying of an aerogel-based coating system in Swedish climates: Field tests and simulations

Ali Naman Karim *, Angela Sasic Kalagasidis, Pär Johansson

Department of Architecture and Civil Engineering, Division of Building Technology, Chalmers University of Technology, SE-41296, Gothenburg, Sweden

A R T I C L E I N F O

Keywords:
Aerogel
Coating mortar
Wind-driven rain
Early stage drying
Retrofitting

A B S T R A C T

Aerogel-based coating mortars (ACM-systems) introduce new solutions for energy-retrofit of uninsulated building envelopes, preserving their characteristics while minimizing the material thickness. However, when introducing new solutions, the long-term durability needs to be investigated. The hygrothermal (heat and moisture) performance is one aspect that needs to be secured. The aim of this study is to investigate the hygrothermal performance, with specific focus on moisture drying, of an ACM-system for external applications in Swedish climates. A field test was conducted where an ACM-system with 40 mm of ACM was applied on the exterior of a brick masonry wall partition. The temperature and relative humidity in the wall were monitored for 15 months. Furthermore, numerical hygrothermal simulations were used to predict the early stage drying and long-term performance of the ACM-system in four Swedish climates. The field measurements showed that the built-in moisture dried out after approximately 6 months, after which the ACM-system followed the variations in the surrounding climate for the remaining period. The simulations predicted that the early stage drying time ranged from 134 to 336 days, depending on climate and time of application. Furthermore, the elevated relative humidity in the ACM due to rainwater absorption resulted in an average thermal conductivity of up to 9 % above the rated value. Consequently, mitigating water absorption at the exterior is crucial for enhancing the long-term thermal performance in high rain load scenarios.

Abbreviations

ACM	aerogel-based coating mortar
ACM-system	coating system with aerogel-based coating mortar
AFR	adhering fraction of rain
RH	relative humidity
WDR	wind-driven rain

* Corresponding author.
E-mail address: ali.karim@chalmers.se (A.N. Karim).

https://doi.org/10.1016/j.jobe.2024.108532
Received 11 September 2023; Received in revised form 22 December 2023; Accepted 12 January 2024
Available online 13 January 2024
2352-7102/© 2024 The Authors. Published by Elsevier Ltd. This is an open access article under the CC BY license (http://creativecommons.org/licenses/by/4.0/).

1. Introduction

Aerogel-based coating mortars (ACMs) can be used either on interior (plaster) or exterior (render) of the load-bearing walls [1]. The declared thermal conductivity of ACMs is 0.03–0.05 W/(m K). This is in the same range as conventional insulation materials such as mineral wool and polystyrene, and less than one tenth of the thermal conductivity of ordinary coating mortars. Commercial ACMs typically consist of a lime and white cement-based binder and gravel aggregate mixed with over 50 vol-% of silica-based aerogel granules. Aerogel is a low-density porous material with thermal conductivities in the range of 0.01–0.02 W/(m K). Finally, ACM products contain additives such as air-entraining and water-repellent agents. Because of the high proportion of porous and fragile aerogel granules, ACMs have lower mechanical strength compared to conventional coating mortars. Consequently, ACMs are often installed in a multilayer coating system (ACM-system) with a few additional layers of ordinary coating mortars to enhance the mechanical stability.

ACMs are primarily intended for retrofitting uninsulated brick and masonry building envelopes to improve energy efficiency [1]. Previous field studies have demonstrated that applying 15–60 mm of ACMs to uninsulated wall elements reduced the U-value by around 30–70 %. Apart from their energy-saving potential, ACMs provide additional retrofitting opportunities for culturally significant structures, where conventional insulation materials are often limiting the application. Renovating such buildings lead to multiple complexities [1–3], including preserving character-defining elements, adhering to permissible building envelope thicknesses, addressing existing moisture-related damage, and avoiding thermal bridges. Using ACMs can overcome some of these challenges while improving energy performance and fulfilling historical preservation requirements.

In the literature, several studies from the period between 2012 and 2021 focused on the thermal performance of ACMs [4–11], while relatively few studies examined their drying performance in the field [1]. In Ref. [12], Stahl et al. reported on the external retrofitting of a historical building in Sissach, Switzerland, by 50–60 mm ACM. Temperature and relative humidity (RH) were measured over a 15-month period. The study showed that the built-in moisture of the ACM had dried out after a few weeks. After that, the construction performed according to expectations. However, to investigate the long-term implications from the initially higher moisture content, several years of measurements were needed [12]. Similar findings were reported by Béjat and Therme [13] who measured the thermal performance of 100 mm ACM applied to the exterior of a brick façade in Le Bourget du Lac, France. During the first 6 months of measurement, the thermal conductivity of the ACM was more than twice the declared dry-state value. This was credited to the higher moisture content in the mortar. As above, the authors recommended a longer monitoring period to determine the final U-value of the wall. Similar recommendations were presented by Fenoglio et al. [14] and Fantucci et al. [15].

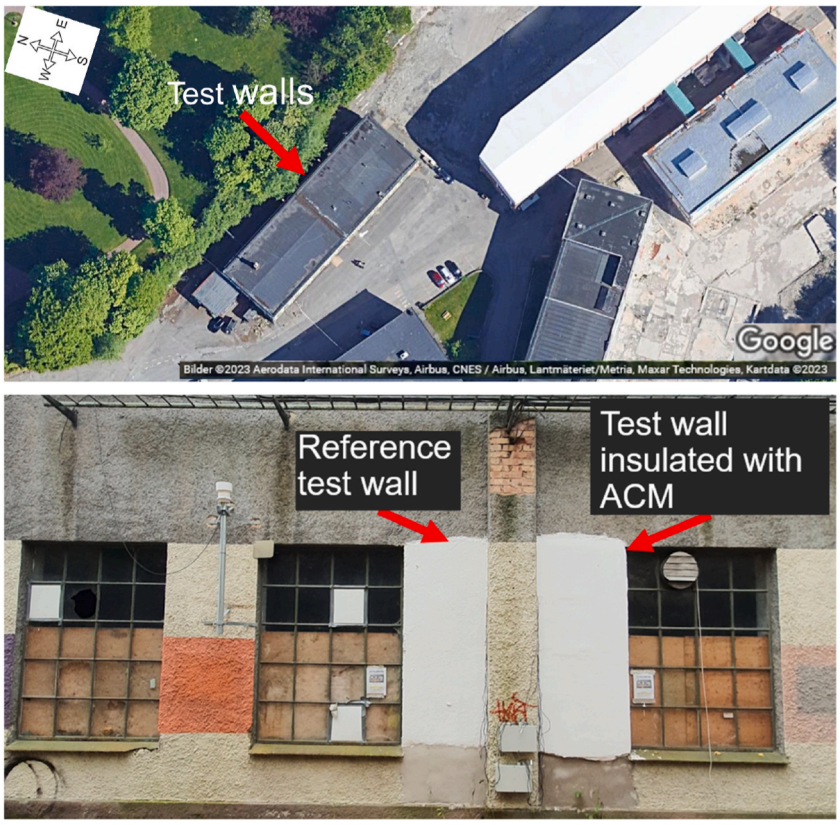

Fig. 1. Top: Overview of the field study building and the tested façade (source: Google Maps). Bottom: Photograph of the wall covered by the ACM-system. The two test walls have a surface area of approximately 3 m^2 each and are located on the northeast façade.

The recommended drying time for ACMs varies for the climate of the location and the chosen internal or external application. Fantucci et al. [16] found that two months was required for the built-in moisture to dry out for an internal application case with 15 mm of ACM in Turin, Italy. A study [17] from Vienna, Austria, of test walls covered with 60 mm ACM with different exterior surface finishing showed that the drying process of the built-in moisture was still in progress 6 months after the ACM application. In a follow-up study of the same walls, Schuss et al. [18] presented the measurement results at the end of two years of measurements. They reported that steady-state conditions was reached after a drying period of around one year and the selection of finishing coating had a minor influence on the hygrothermal performance and drying of the ACM [18].

Existing field studies predominantly focus on predicting the drying performance of ACM-systems in Central European conditions, leaving a notable research gap for Swedish climates. Southern and western regions of Sweden, with subpolar oceanic climates (Cfb) [19], encounter high humidity and frequent wind-driven rains (WDRs), leading to elevated moisture loads. Unlike other explored locations, these conditions pose challenges for moisture removal and necessitate testing of ACM-systems in local climates. This approach is crucial for developing moisture-safe designs and facilitating thermal performance of these systems in real-life scenarios.

This paper addresses the identified knowledge gaps by assessing 1) the early stage drying of built-in moisture, and 2) the long-term hygrothermal performance of a commercially available ACM-system within the context of Swedish climates. The investigation incorporates both field tests and numerical hygrothermal simulations. The paper is structured as follows: Chapter 2 outlines the studied ACM-system, field measurements and hygrothermal simulations. Chapter 3 discusses the compiled results, while Chapter 4 presents conclusions from the conducted studies.

2. Materials and methods

ACM-systems incorporate larger thicknesses and longer drying times than ordinary coating mortars. To gain deeper insights in the drying process, a field test was conducted to study the drying of a commercially available ACM and an ordinary coating mortar. While the field test covered one wall with specific conditions, numerical hygrothermal simulations were employed to explore diverse locations and weather exposures, including high rainfall scenarios. The model's accuracy was verified against experimental field test results.

2.1. Field measurements

The field test took place in Gothenburg on the southwest coast of Sweden, focusing on a section of the northeast wall of a masonry brick building from 1921. A commercially available ACM-system covered approximately 3 m^2 of the wall, as shown in Fig. 1. Adjacent to it, a wall section of similar size was coated with a conventional lime and cement-based coating mortar. Both wall partitions were externally covered by a white, water-repellent paint. The selection of the northeast wall and a 3 m^2 surface area was based on practical, economic, and temporal constraints (more in Discussions).

Fig. 2 illustrates the layer arrangement and approximate thicknesses of the ACM-system, following the widely accepted design [1]. The application process involved individual layers, with each layer drying before the next was added. The sequence included an undercoat for improved adhesion, a 40 mm ACM layer, a primer, and an outer coating mortar with mechanical strength provided by a glass fiber reinforcement mesh. After drying, a second layer of outer coating mortar was applied. The system was completed with a mineral-based (silicon) vapor-open, water-repellent paint for desired surface properties and appearance. The ACM-system on the test wall measured approximately 50 mm in total thickness, while the conventional mortar on the reference wall was about 10 mm thick. Declared properties of both the ACM-system [20] and of the conventional coating mortar [21] are summarized in Table 1.

Table 2 details the layer thicknesses and recommended drying times for the ACM-system, while Fig. 3 outlines the application steps. The application phase spanned over two months, concluding in December 2021. To shield the mortars walls from adverse weather conditions during curing, including low temperatures (below 5 °C), rain, wind, and solar radiation, weather protection and an electrical radiator were used, following the producer's recommendations (Fig. 3a). Due to the smaller size of the test wall partition compared to the original façade, precautions were taken at intersections to address potential surface boundary effects. This involved applying extra coating mortar and water-repellent paint to the edges, reducing the risk of rainwater infiltration.

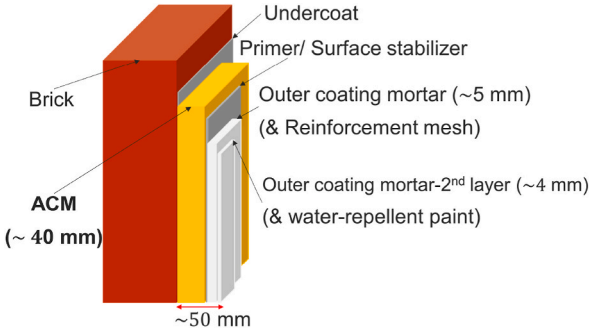

Fig. 2. Schematic representation (not to scale) of the ACM- ACM-system, as per standard practice [1]. The sequence included an undercoat for improved adhesion, a 40 mm ACM layer, a primer, and an outer coating mortar with mechanical strength provided by a glass fiber reinforcement mesh. The total thickness of the ACM-system was about 50 mm.

Table 1
Selection of declared material properties of the main layers in the ACM-system [20] and of the conventional coating mortar used in the reference test wall [21].

	Test wall		Reference wall	Test & Reference wall
Material property	ACM	Outer coating mortar	Conventional coating mortar	Water-repellent paint
Density, ρ (kg/m^3)	180	1200	–	–
Thermal conductivity, λ_{dry} (W/(m·K))	0.04	0.9	0.6	–
Water vapor permeability coefficient, μ-value (–)	≤ 5	10	≤ 11	s_d[a] = 0.01 m
Water absorption coefficient, A_{cap} (kg/(m^2·min$^{0.5}$))	≤ 0.2	≤ 0.4	W_c0: no specified value	0.01–0.06
Compressive strength, σ_c (N/mm^2)	0.5	1.3	CS II: 1.5–5.0	–

[a] – A s_d - value of 0.01 m corresponds to a vapor resistance of 0.01-m-thick layer of stagnant air.

Table 2
Thickness and minimum drying time of each layer in the ACM-system.

Layers in the ACM-system	Thickness (mm)	Minimum drying time (days)
Undercoat	–	1
ACM	40	28
Primer	–	1
Outer coating mortar (and mesh)	5	5
Outer coating mortar (second layer)	4	14[a]
Water-repellent paint (three steps)		
Primer	–	1
Paint	–	1
Paint (second layer)	–	1
Total	50	52

[a] According to the manufacturer's recommendation, a minimum duration of 14 days is necessary before removing weather protection or applying paint.

Fig. 3. Application steps for the ACM-system, including a) Weather protection used during the application phase to prevent weather induced stresses. The process involved b) Preparation, removal of the existing coating mortar, and cleaning of the substrate, c) Application of undercoat/base mortar, d) ACM, and e) A first layer of outer mortar with reinforcement mesh, f) Final appearance of the test wall after removal of the weather protection.

To monitor the hygrothermal performance of the test wall, temperature and relative humidity (RH) sensors were placed at various depths and heights as shown in Fig. 4. In the test wall, sensors were placed at three depths: in the middle of the existing brick wall (P1), behind the ACM (P2), and behind the outer coating mortar (P3). For the reference wall, sensors were placed at two depths: in the middle of the existing brick wall ($P1_{ref}$), and behind the conventional coating mortar ($P2_{ref}$). Each position had three sensors at different heights (up, middle, down) with around 500 mm spacing. The sensors were so called Sahlén sensors which have a piece of

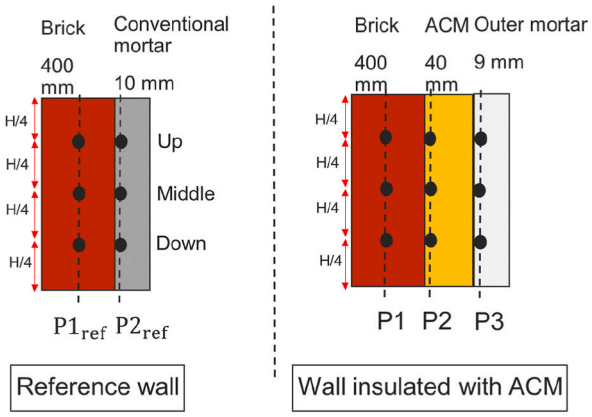

Fig. 4. Schematic (not to scale) illustration of the placement and labeling of sensors in the reference test wall (left) and the one covered by ACM-system (right). Three sensors were placed evenly at each position with respect to the height (H) of the test walls: up, middle, and down. Both test walls were coated externally with white water-repellent paint. Images of the sensors in positions P2 and P3 are displayed in Fig. 3c and d, respectively.

birch wood (diameter: 13 mm, Length: 40 mm) where the moisture is measured by a Protimeter Timbermaster Bollmann HDI 3.1. The sensors measured temperature and RH in the range of −20 °C–60 °C and 60 %–100 % RH. Outdoor air temperature and RH were also recorded by a protected sensor near the wall. All sensors exhibited a measurement accuracy of ±2.5 % in the 10 %–90 % RH range and ±0.5 °C at 25 °C. The measurement interval was set to 10 min, with hourly averages and seven-day moving averages calculated.

The measurements covered a 15-month period, from January 1, 2022 to March 31, 2023. The selected duration encompassed a full year of data collection, with an additional three months. This extended duration allowed for a full year of data collection, with an additional three months to distinguish the influence of the early stage drying from the outdoor climate impact on recorded RH in the test walls. This distinction was achieved by comparing RH levels during the initial three months with those in the concluding three months of the monitoring period.

A WTB100 tipping bucket rain gauge [22], with a collecting volume of 200 cm^3 and ±2 % accuracy, measured on-site rainfall intensity. The gauge generated a pulse signal when filled, registering rainfall only when the 200 cm^3 volume was reached. The test wall, shielded from WDR by trees and a nearby wall (Fig. 1), were primarily exposed to vertical rainfall and runoff.

Interior climate monitoring was restricted by tenant limitations. However, as the building remained mostly vacant during the 15-month measurement period from January 1, 2022, to March 31, 2023, the interior climate was influenced by outdoor conditions rather than consistent heating. Both the test and the reference wall partitions experienced the same interior climate conditions.

2.2. Hygrothermal simulations

To study the ACM-system drying at other weather conditions than those covered in the field test, a widely recognized building physics software WUFI 2D 3.4 [23] was utilized. With reasonable assumptions about material properties and indoor/outdoor climate conditions, WUFI provides accurate estimates of long-term hygrothermal performance and drying duration for building envelopes. WUFI has been used and verified in previous studies, effectively addressing coupled heat and moisture transfer in walls with ACM-systems [6,12,23,24]. Using the finite volume technique and implicit scheme for spatial and temporal discretization, WUFI considers temperature and relative humidity as driving potentials for heat and moisture transport [25]. The software calculates liquid water transport based on moisture content, suction coefficient D_{ws} (m^2/s), and redistribution coefficient D_{ww} (m^2/s). Essentially, D_{ws} describes the capillary water uptake in the event of rain while D_{ww} describes the moisture redistribution when rain is absent. As

Table 3
Thickness and material properties of the layers in the simulated construction in WUFI [26].

	Brick masonry	ACM		Outer coating mortar
Thickness (mm)	400	40		9
Vapor permeability, μ-value (−)	10[e]	3[a]		10[d]
Water absorption coefficient, A_{cap} (kg/(m^2·$min^{0.5}$))	0.85[e]	0.04[b]		0.08[b]
Thermal conductivity, λ (W/(m·K))	λ_{dry}: 0.6[e]	RH (%)	λ[c]	λ_{dry}: 0.9[d]
		0	0.04	
		80	0.045	
		90	0.05	
		100	0.4	

Measured in the laboratory.
[a] - EN 1015–19 [27].
[b] – EN 1015–18 [28].
[c] – ISO 22007–2 [29].
[d] : Declared value [20].
[e] : From WUFI database.

measured values for these coefficients are limited, WUFI utilizes a simplified approximation method based on material properties, A_{cap} ($kg/m^2 \cdot s^{0.5}$), w (kg/m^3), and free water saturation w_f (kg/m^3), as expressed in Eq. (1).

$$D_{ws} = 3.8 \bullet \left(\frac{A_{cap}}{w_f}\right)^2 \bullet 1000^{\frac{w}{w_f}-1} \quad (1)$$

The adhering fraction of rain (AFR), a unitless parameter in WUFI, specifies the proportion of rainwater striking the façades and available for capillary water absorption. AFR is defined as 1 when all rainwater is available for absorption and 0 when no capillary absorption occurs. For moderately exposed façades, a value of 0.7 is recommended [25].

2.2.1. Model verification

To verify the simulation model, the measured RH at sensor positions P1 and P2 (Fig. 4) was compared to the simulated results. The construction layers' thickness and material properties were adopted from the test wall with the ACM described in Chapter 2, as presented in Table 3 and Fig. 5. Two parameters were unknown: the interior climate and material properties of the existing brick wall. These were determined through a parametric pre-study detailed in Appendix A. The brick type "brick masonry" was chosen based on the best agreement with the field measurements. To represent the water-repellent paint, an additional vapor resistance, with a s_d -value of 0.01 m [20], was applied on the exterior boundary surface.

A time step of 1 h was used in all simulations, and the built-in meshing function in WUFI was used to discretize the space domain utilizing structured grids of rectangular elements. A mesh convergence analysis was conducted to ensure the meshing did not impact the simulated output. The number of elements in each material layer was iteratively increased until meeting a convergence criterion. This criterion was defined by the total moisture content within the individual material layers and the entire construction. Mesh refinement proceeded iteratively until the deviation in the moisture content, in relation to the preceding refinement step was less than 1 %.

The hygrothermal model details are presented in Table 4, with initial conditions set to the beginning of the measurement period (January 1, 2022) and outdoor climate based on measured values in the field test. The solar radiation was not considered due to the test wall's orientation and shading from sun. The exterior and interior surface heat transfer coefficients were set to 25 and 8 $W/(m^2 \cdot K)$ [31], respectively. The simulations assumed a test wall free of damage and water leakage, with the AFR set to 0 for model verification analyses. The interior climate was determined based on the pre-study detailed in Appendix A. The interior temperatures were assumed to be 5 °C higher than the exterior air temperatures due to the thermal inertia of the building, solar radiation, and the assumed additional heating. Based on this assumption, the interior relative humidity was calculated assuming no interior moisture supply.

2.2.2. Early stage drying

In this study, the early stage drying period is defined as the time required for the built-in moisture in the initially wet and saturated ACM to reach a RH of 70 % behind the ACM. The drying cycle was completed when the 70 % RH threshold was reached and maintained below 80 % RH for a minimum of 30 consecutive days at position P2 (Fig. 4). This drying criterion was selected as a conservative threshold considering the moisture-dependent thermal conductivity of the ACM (Table 2). The increase in thermal conductivity remains below 13 % up to 80 % RH, beyond which the increase becomes more substantial. Previous studies [6,12] on other ACM products have also demonstrated significant impact of moisture on the thermal conductivity, exceeding a 30 % increase for RH levels higher than 60–80 %.

The simulation model described in Section 2.2 was evaluated by comparing the simulated drying time for the ACM in the field test to the measured drying time. The drying time if the building had been heated (according to the EN 15026 [31]) was also calculated. Furthermore, the same simulation model with the same construction as in the field test was used to calculate the early stage drying time

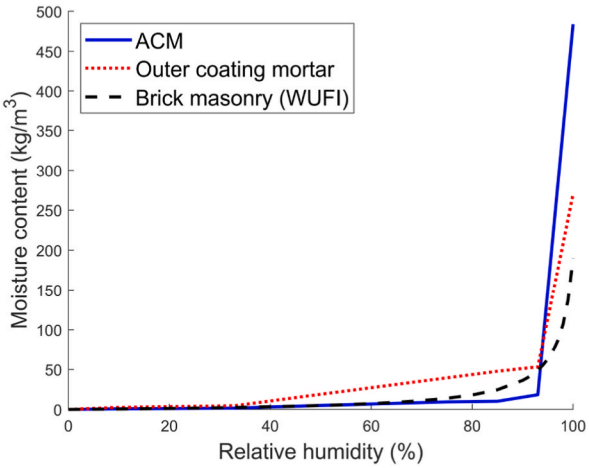

Fig. 5. Moisture sorption isotherm of the materials used in the simulations. For brick masonry, the graph was extracted from the WUFI database [26]. For the ACM and outer coating mortar, the adsorption curves were extracted from Ref. [30] measured in the laboratory according to EN 1015–18 [28].

Table 4
Model specifications used in the verification study.

Exterior surface heat transfer coefficient	25 W/(m^2·K)
Interior surface heat transfer coefficients	8 W/(m^2·K)
Initial condition (RH)	RH_{brick} = 78 %, RH_{ACM} = 99 %, $RH_{outer\ mortar}$ = 80 %
Short-wave radiation absorptivity	0 (−)
Long-wave radiation absorptivity	0 (−)
Exterior climate	Exterior air temperature and relative humidity measured in the field
Interior climate	Interior air temperature estimated to 5 °C higher than the exterior temperature. The indoor relative humidity is adjusted to the indoor temperature, assuming the same moisture content indoors and outdoors.
Water-repellent paint (exterior)	s_d - value: 0.01 m
Orientation	Northeast
AFR	0 (−)

of the ACM for different climate conditions in Sweden. Four Swedish cities, Gothenburg (west coast), Stockholm (east coast), Östersund (middle), and Kiruna (north), were selected. The built-in weather data files in WUFI were considered with typical values over a period from 1995 to 2005. This dataset has been used in several previous studies on long-term performance of ACM-systems [6,12,23,24]. Most importantly, it encounters the period of recent climate changes in Sweden, characterized by warmer and more humid climates. Table 5 provides an overview of the weather conditions in the four cities.

To investigate the influence of the time of application on the early stage drying time of the ACM, four different times of application were considered for each of the four cities. The drying was initiated on January 1st, March 1st, June 1st, and September 1st, respectively. The specified details of the simulation model are presented in Table 6. The initial moisture content in the coating system was assumed to be wet and saturated, while the brick wall was assumed to have an average RH of 80 %. The orientation of the test wall was set to north with the lowest drying potential for all four cities. The short-wave and long-wave radiation absorptivity coefficients were set to 0.2 and 0.9, respectively. The interior climate was assumed to be heated according to EN 15026 [31]. A leakage-free construction and a fully water-repellent paint were assumed on the exterior, resulting in an AFR of 0.

2.2.3. *Long-term hygrothermal conditions*

The long-term performance of the ACM-system was investigated by hygrothermal numerical simulations. The construction in the field was modelled with the data described in Chapter 2. The analyses were performed for the cities in Table 5 with model specifications as in Table 7. Two scenarios were defined for the long-term analyses based on the orientation of the test wall: 1) oriented towards the direction of prevailing WDR, 2) oriented towards the minimum drying potential i.e., lowest solar radiation exposure. Two cases were considered for each scenario, with AFR values of 0 (no rain) and 0.7 (moderately exposed), respectively. In all simulations, a moisture source was defined at the interface between the ACM and brick. It corresponded to 1 % of the WDR on the exterior surface, as recommended in the ASHRAE Standard 160 [32], representing additional water penetration through cracks or window joints. With respect to the moisture source, the 1D model used so far was shifted to a 2D model representing a 1-m-high test wall. The source was defined in the middle of the wall in the vertical direction, with both a width and height of 10 mm.

To reach steady-state conditions, the simulations were performed for five consecutive years using the same weather data repeatedly. The long-term moisture drying and the risk for moisture accumulation of the studied test wall with ACM were studied by evaluating the total moisture content, w_{tot} (kg/m^3). In addition, the RH behind the ACM at position P2 (Fig. 4) and the average RH in the ACM layer were evaluated. The expected thermal conductivity of the ACM in the field was calculated using the moisture-dependent thermal conductivity of the ACM (Table 3) and the overall RH level in the ACM.

Table 5
Overview of the weather conditions in the four cities considered for hygrothermal simulations, based on the weather data file in WUFI [26].

	Gothenburg	Stockholm	Östersund	Kiruna
Köppen−Geiger Climate Classification [19][a]	Cfb	Dfb	Dfc	Dfc
Temperature (°C)				
Maximum	27.8	29.4	27.2	25.1
Average	8.8	6.8	1.5	−1.7
Minimum	−12.2	−18.6	−39.0	−41.4
Relative humidity (%)				
Maximum	94	99	99	96
Average	74	79	80	77
Minimum	19	22	18	23
Prevailing direction of WDR	South	Southeast	East	North/South
Average wind velocity (m/s)	2.97	3.13	2.08	3.14
Accumulated rain load (mm/year)	1074	639	502	533

[a] Cfb: Temperate climate, fully humid, warm summer. Dfb: Snow climate, fully humid, warm summer. Dfc: Snow climate, fully humid, cool summer, and cold winter.

Table 6
Model specifications used to predict the early stage drying period of the ACM-system in four Swedish cities.

Exterior surface heat transfer coefficient	25 W/(m^2·K)
Interior surface heat transfer coefficients	8 W/(m^2·K)
Initial condition (RH)	RH_{brick} = 80 %, RH_{ACM} = 99 %, $RH_{outer\ mortar}$ = 99 %
Short-wave radiation absorptivity	0.2 (−)
long-wave radiation absorptivity	0.9 (−)
Exterior climate	WUFI data file [26] for the considered city
Interior climate	EN 15026
Water-repellent paint (exterior)	s_d - value: 0.01 m
Orientation	North
AFR	0 (−)

Table 7
Scenarios and model specifications used for the long-term hygrothermal analyses on the ACM-system.

Exterior surface heat transfer coefficient	25 W/(m^2·K)
Interior surface heat transfer coefficients	8 W/(m^2·K)
Initial condition (RH)	80 % (1st January)
Short-wave radiation absorptivity	0.2 (−)
long-wave radiation absorptivity	0.9 (−)
Exterior climate	WUFI data file [26] for the considered city
Interior climate	EN 15026
Water-repellent paint (exterior)	s_d - value: 0.01 (−)
Height of the test wall	1 m
Scenario 1	
Orientation	The prevailing direction of WDR for the considered city (see Table 5)
AFR	0 and 0.7 (−)
Moisture source/Leakage	1 % of WDR: at the interface between the ACM and brick
Scenario 2	
Orientation	North: the direction with minimal solar radiation exposure
AFR	0 and 0.7 (−)
Moisture source/Leakage	1 % of WDR: at the interface between the ACM and brick

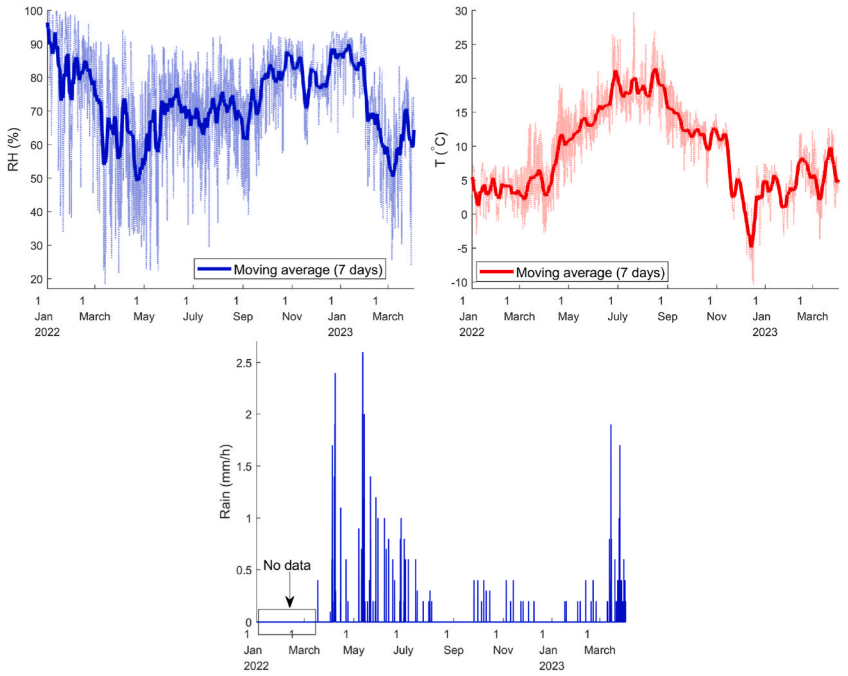

Fig. 6. Top: Hourly average and seven-days moving average of the outdoor air temperature and relative humidity in the field. Bottom: Hourly average rain intensity. Rain data was missing between 2022 and 01-01 and 2022-03-16 due to sensor malfunction.

3. Results and discussion

Sections 3.1 and 3.2 present and discuss the results of the field measurements and hygrothermal simulations, respectively.

3.1. Field measurements

Fig. 6 displays the hourly average and seven-day moving average of the field-measured outdoor temperature, RH, and rain intensity. Outdoor temperatures ranged between −10 °C and 30 °C, averaging around 9 °C, with RH ranging from 18 % to 100 %, averaging approximately 73 %. These values align with historical weather data for Gothenburg (Table 5). The recorded maximum rain intensity was 2.6 mm/h, accumulating to about 120 mm during the study, notably lower than the historical average of 1074 mm/year (Table 5). A comparison with data from the Swedish Meteorological and Hydrological Institute (SMHI) weather station in Gothenburg, reporting 577 mm rainfall in 2022 [33], further underscores these findings.

Fig. 7 displays the seven-day moving average of the measured RH for both the reference wall and the wall insulated with ACM-system. The low temperature gradient across the wall, attributed to an unheated interior, meant that RH was predominantly influenced by the construction moisture content.

The RH in the wall with ACM indicated that the built-in moisture in the initially wet ACM underwent drying within approximately six months. Over this period, moisture was partly redistributed from the wet ACM-system to the brick wall (from P2 and P3 to P1), resulting in increased RH in the brick and decreased RH in the coating system. A similar drying trend and moisture redistribution was observed for the reference wall, albeit with a relatively higher drying rate. The thickness of the ACM-system (around 50 mm) was five times greater than that of the conventional coating mortar (10 mm), potentially explaining the longer drying time for the former. The RH behind the outer coating mortar (P3) and the conventional mortar in the reference wall (P2ref), both with a thickness of approximately 10 mm, exhibited a comparable drying rate. Once the built-in moisture of the ACM-system dried out, the RH in the test wall (P1–P3) closely followed the RH in the outdoor air. Consequently, no signs of moisture accumulation were observed in the ACM-system during the initial 15 months of measurement.

As mentioned in Section 2.1, the field test was conducted on two smaller wall partitions, each with an approximate surface area of 3 m^2, on the northeast-oriented façade. Although a larger test area would have been desirable, practical limitations, such as time and economic constraints, made this unfeasible. Testing on a south-oriented façade (the prevalent direction of WDR) was not possible due to the layout of the building.

Preliminary hygrothermal simulations prior to the field test indicated that the façade size adequately established one-dimensional conditions for heat and moisture transport. Potential boundary effects at the intersection between the test wall partition boundaries and the original brick façade were constrained to local temperature and relative humidity at the edges, not impacting the central parts where sensors were positioned. Furthermore, as detailed in Section 2.1, additional coating mortar and water-repellent paint were applied along the edges to mitigate boundary effects, specifically addressing concerns like rainwater intrusion from the edges into the test walls.

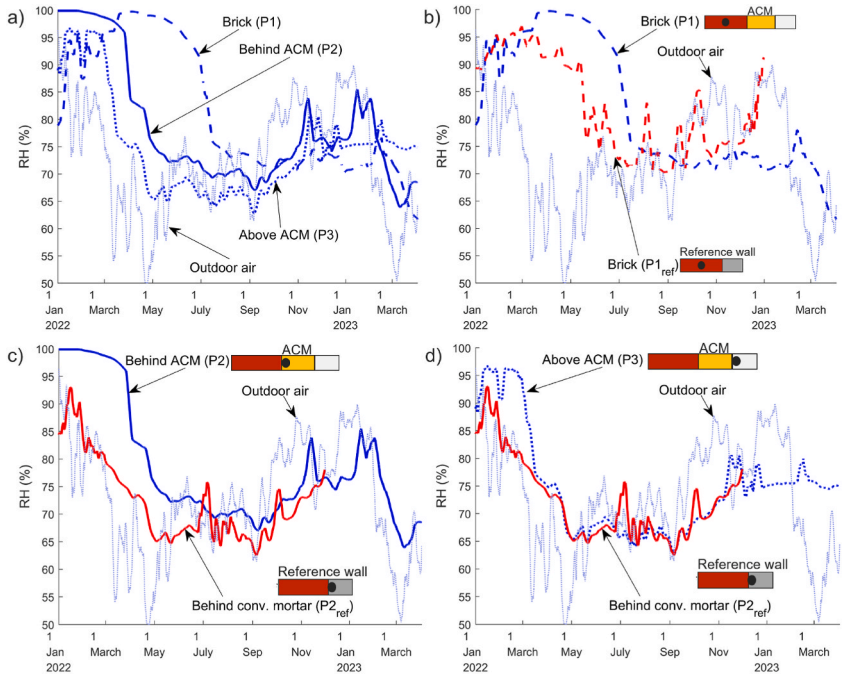

Fig. 7. Seven-days moving average of measured RH at the different positions in the reference wall and the wall insulated with ACM. RH values are averaged from three sensors (up, middle, down). a: RH in the wall insulated with ACM. b, c, d: Comparison between the RH in the test wall and the reference wall.

The maximum variation in RH among the three sensors at each layer ranged within 3–11 %. Prior to the field test, the sensors' measurement accuracy (declared accuracy of ±2.5 % at 10–90 % RH) underwent further laboratory verification for RH between 90 and 100 %, demonstrating a verified accuracy within ±2.5 %. Despite this, the sensors exhibited varying response delays after RH changes, spanning from a few hours up to three days. Notably, the moisture sensors with birch probes displayed different moisture capacity compared to the ACM and other materials in the test walls, potentially explaining the disparate response times to changes in surrounding RH. To address these variations in sensor response times, the analyses considered the seven-day moving average of the measured values.

3.2. Hygrothermal simulations

3.2.1. Model verification

Fig. 8 illustrates the simulated and measured RH and temperature in the brick (P1) and behind the ACM (P2). As discussed earlier regarding the negligible temperature gradient over the wall, Fig. 8 (c, d) verifies minimal temperature variations between P1 and P2. The maximum temperature difference observed was 4 °C, with an average difference of 0.5 °C.

As shown in Fig. 8 (a, b), the simulations mirrored the observed trend of moisture redistribution as in the measurements, leading to an increase in RH in the brick during the initial six months of early stage drying. However, the simulated RH values were on average 7% units lower than the measured values during this period. From July onward, a closer agreement was attained between the measured and simulated RH in the brick (P1). Similar patterns were noted in the comparison between the measured and simulated RH at P2, located behind the ACM. In the initial six months, the average difference between the simulated and measured RH was 7% units. The simulations demonstrated improved alignment with the measured values for the remaining measurement period. A steep decline in RH was observed around 90 days in the measurements (P2), while the simulations predicted a similar decline with a time lag of approximately 50 days. The measured RH at P2 reached 70 %, the threshold for early stage drying completion, after 191 days, while the simulated RH achieved the same after 192 days.

The verification study demonstrated that the simulation model accurately predicted the total duration of the early stage drying, despite the initial deviation between the simulated and measured RH. The satisfactory agreement observed between the measured and simulated RH after the early stage drying period indicates the model's reliability in assessing the long-term performance of the ACM-system.

The parametric study in Appendix A suggested that factors such as the choice of brick type, interior climate, and water absorptivity of the ACM and outer mortar in the simulations, did not fully account for the observed discrepancy between the simulated and measured values during the initial drying months. A combination of these acknowledged uncertainties, measurement errors, and differing response times of the sensors could potentially elucidate the observed differences.

3.2.2. Early stage drying

The early stage drying period was defined as the time required to attain a maximum RH of 70 % behind the ACM, maintaining RH below 80 % for at least 30 consecutive days. In the field, this drying period spanned 191 days. The simulations, assuming a five-degree higher temperature inside than outside, predicted a drying period of 192 days. The simulations also indicated a shorter drying time of 137 days if the interior was heated according to EN 15026 [31].

Fig. 9 presents the predicted duration of the early stage drying for the ACM in four Swedish cities at four different times of application. Results revealed a drying period ranging from 134 to 336 days. The longest drying time occurred in Stockholm in September, while the shortest drying time corresponded to an application in Kiruna in September. For Gothenburg and Stockholm, the shortest and longest drying times were projected for drying commencing in June and September, respectively. In Östersund and Kiruna, the same corresponded to September and January, respectively.

The investigation of the early stage drying of the ACM in four Swedish cities revealed that the drying period was influenced by location, climate, and time of application. Variations between cities were attributed to seasonal weather disparities. The chosen criterion of achieving 70 % RH behind the ACM could also explain the variation in results between the cities, and an alternate criterion might yield different outcomes. Nevertheless, the estimated number of drying days highlights the most advantageous time for ACM application in four distinct Swedish climates.

3.2.3. Long-term hygrothermal performance

This section presents the simulation results for the long-term hygrothermal performance of the externally insulated test wall with ACM-system. To improve the readability, scenario 1 (test wall oriented towards the prevailing direction of WDR), resulting in more extreme conditions, is discussed here. Results for scenario 2 (north-oriented test wall) are compiled in Appendix B.

Fig. 10 depicts the w_{tot} in the ACM-insulated test wall at various locations over five years of simulations. The outcomes suggest a dynamic steady state was achieved after approximately 1.5–2 years for both cases with assumed AFR of 0 (no rain) and 0.7 (rain). With no rain absorption, the highest w_{tot} at steady state occurred in Gothenburg (6.5 kg/m^3), about 23 % higher than the maximum w_{tot} in Kiruna (5.3 kg/m^3). Conversely, for scenarios with rainwater absorption, the maximum w_{tot} in Gothenburg reached up to 15.3 kg/m^3, more than twice as high as in Kiruna (7.5 kg/m^3). These results suggest that the ACM-system could dry out in all locations without moisture accumulation over an extended period.

Fig. 11 illustrates the RH during the last year of the five-year simulation, at the interface between ACM and brick (P2) in the four Swedish cities. Without rain, comparable RH ranging from 35 to 60 % were obtained in Gothenburg and Stockholm, while lower RH ranging from 25 to 60 % and 20–57 % were obtained in Östersund and Kiruna, respectively. In scenarios with rain, RH generally increased for all four cities, with the highest increase in Gothenburg followed by Stockholm. RH in Gothenburg varied between 52 and

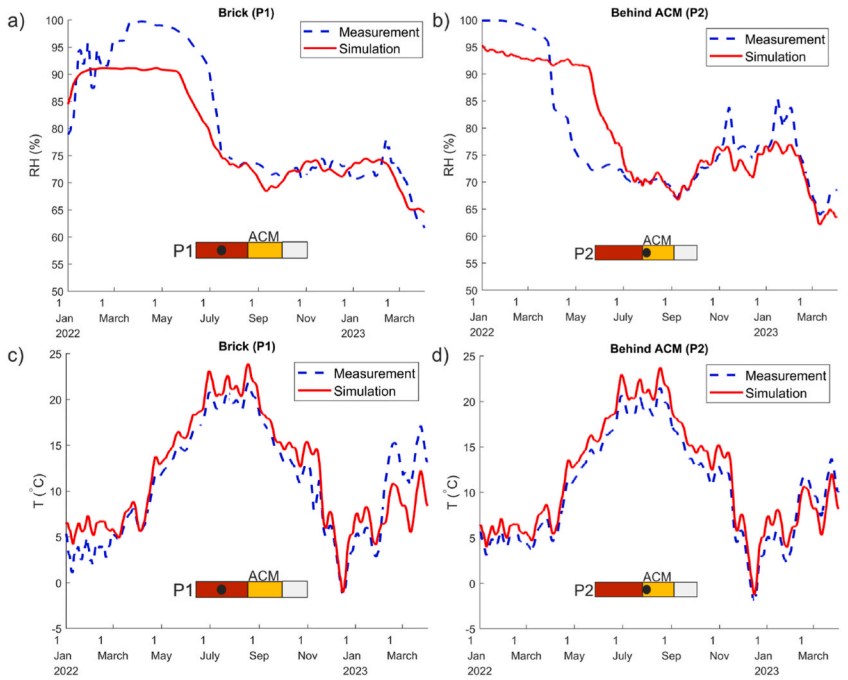

Fig. 8. Simulated and in-field measured values (seven-days moving average) of RH (a, b) and temperature (c, d) in the brick (P1, left) and behind the ACM (P2, right).

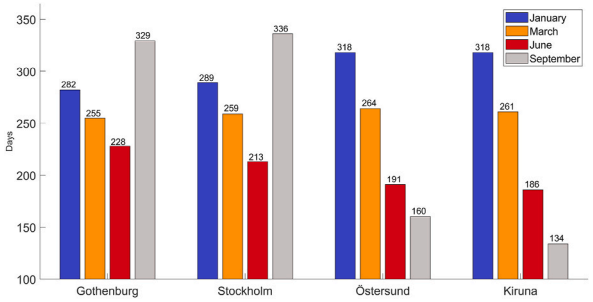

Fig. 9. Simulated duration of early stage drying time for the four Swedish cities and the four times of application.

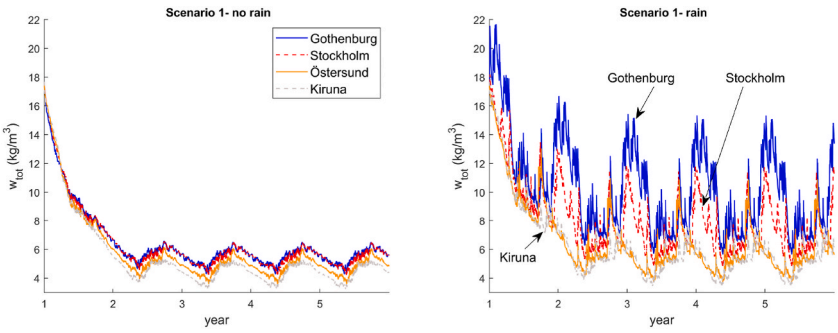

Fig. 10. Simulated water content in the test wall with ACM-system in various locations. Left: No rain. Right: Rain.

81 %, while it ranged from 46 to 72 % in Stockholm. For Östersund and Kiruna, RH varied between 29-70 % and 24–67 %, respectively. These results indicate that, with or without rainwater absorption at the exterior, the risk of condensation at the ACM-brick interface could be eliminated in all locations, as RH never exceeded 81 %.

Fig. 12 presents the average RH and the corresponding thermal conductivity of the ACM for each of the four cities. For the case

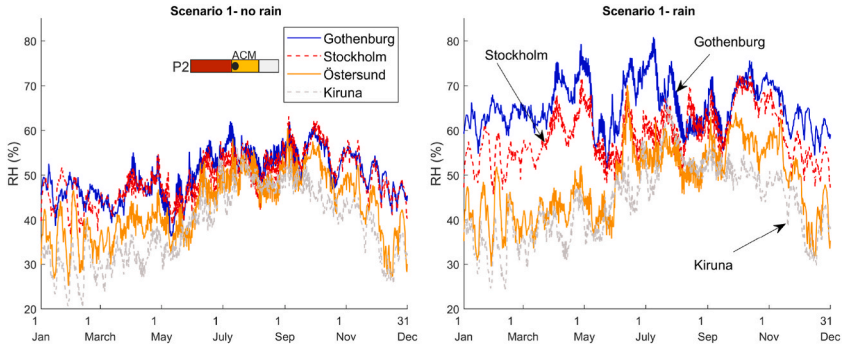

Fig. 11. Simulated RH at the interface between the ACM and brick (P2), corresponding to the last year of simulations for all four cities. Left: No rain. Right: Rain.

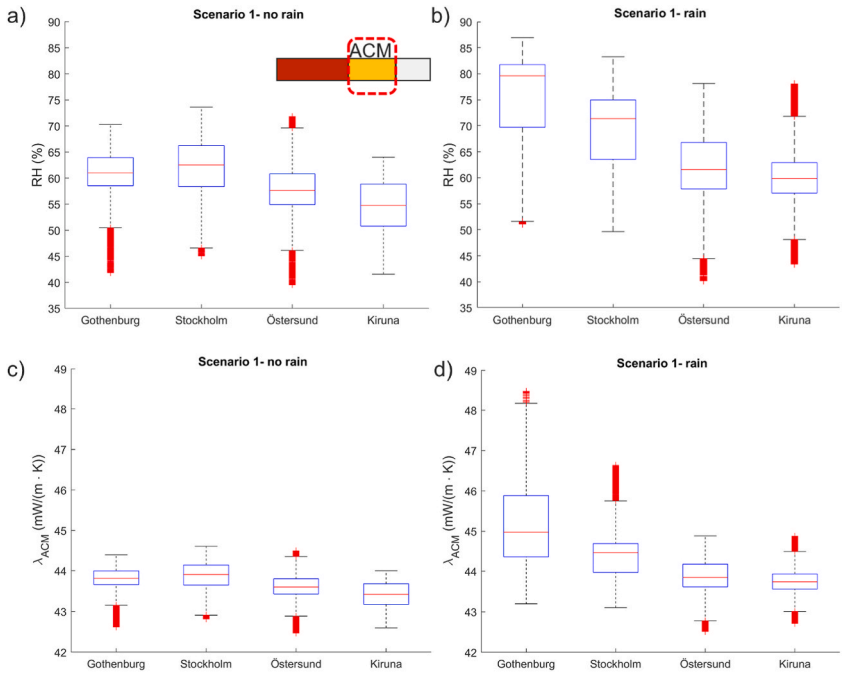

Fig. 12. A,b: Simulated average RH in the layer of ACM. c,d: Calculated moisture-dependent thermal conductivity of the ACM. Left-no rain. Right-rain.

without rainwater absorption, the average RH ranged from 40 % (Östersund) to 74 % (Stockholm). The median RH in Stockholm (highest) was around 14 % higher than the median RH in Kiruna (lowest). For the case with rainwater absorption, the RH ranged from 40 % (Östersund) to 87 % (Gothenburg), and the median RH in Gothenburg (highest) was around 33 % higher than in Kiruna (lowest).

The results indicate that when rainwater absorption is mitigated, the RH of ACM remains below 80 %, resulting in a lower thermal conductivity. As illustrated in Fig. 12c, the moisture-dependent thermal conductivity of the ACM was approximately 0.042–0.045 W/(m·K). However, with rainwater absorption (Fig. 12d), the thermal conductivity of the ACM increased by up to 9 % to 0.042–0.049 W/(m·K). In Gothenburg, where the WDR load on the test wall was the highest, the median thermal conductivity was approximately 3 % higher for the case with rainwater absorption compared to the complete elimination of rainwater absorption.

4. Conclusions

The study investigated the early stage drying and long-term hygrothermal performance of an aerogel-based coating mortar (ACM-system) for external applications in Swedish climates. A field test conducted in Gothenburg, Sweden, involved two northeast-oriented test wall partitions—one coated with an ACM-system (40 mm of ACM) and the other with a 10 mm conventional coating mortar. Monitoring of the temperature and moisture conditions at various depths and heights occurred over the initial 15 months. Numerical hygrothermal simulations predicted the hygrothermal performance of the ACM-system in four Swedish cities of Gothenburg (west coast), Stockholm (east coast), Östersund (middle), and Kiruna (north).

The field test showed that the built-in moisture in the ACM required approximately six months to dry out, with no observed

moisture accumulation in the ACM-system over the 15-month monitoring period. Simulated early stage drying durations in the four cities ranged from 134 to 336 days. The shortest and longest drying times occurred in Gothenburg and Stockholm for applications in June and September, respectively. In Kiruna and Östersund, the shortest and longest drying times were in September and January, respectively. The long-term simulations showed that the ACM-system dried out and subsequently aligned with the ambient climate. However, rainwater absorption at the exterior surface increased the overall relative humidity in the ACM, resulting in a higher average thermal conductivity, up to 9 %. Therefore, for walls exposed to wind-driven rain, the rainwater absorption at the exterior should be limited to improve the thermal performance of the ACM.

The outcomes of the study offer valuable insights for designing external retrofitting of buildings in Swedish climates utilizing ACM-systems. The findings suggest that an early stage drying period of up to approximately one year can be anticipated, resulting in reduced thermal performance of the ACM-system during this interval. For long-term considerations and pay-back time estimations of external retrofitting with ACM-systems, it is advisable to factor in a higher thermal conductivity, up to 9 %, compared to the declared values measured in the laboratory and under dry conditions. Future research should consider extended monitoring periods, particularly at highly exposed façades to wind-driven rain, to enhance the precision of predictions regarding the long-term performance of ACM-systems.

CRediT authorship contribution statement

Ali Naman Karim: Conceptualization, Data curation, Formal analysis, Investigation, Methodology, Software, Validation, Visualization, Writing – original draft, Writing – review & editing. **Angela Sasic Kalagasidis:** Conceptualization, Supervision, Writing – review & editing. **Pär Johansson:** Conceptualization, Funding acquisition, Project administration, Supervision, Writing – review & editing.

Declaration of competing interest

The authors declare that they have no known competing financial interests or personal relationships that could have appeared to influence the work reported in this paper.

Data availability

Data will be made available on request.

Acknowledgment

The authors would like to acknowledge the Swedish Energy Agency for financial support (project 46822–1 & P2022-00872), and to Mölndala Fastighets AB for their valuable contribution in conducting the field test.

Appendix A. Hygrothermal simulation model verification

In the following, the outcomes of a parametric study focused on evaluating the influence of various factors on the simulation results are presented. These included the properties of the brick in the test wall and the interior climate conditions in the field. Furthermore, a sensitivity analysis was conducted to evaluate the impact of the water absorption coefficient (A_{cap}) of both the ACM and the outer coating mortar. All simulations adhered to the model detailed in Section 2.2.1. The results for each investigated case were compared to the corresponding measurement outcomes in the executed parametric analysis.

Brick type

Table A 1 presents the hygrothermal properties of four different brick types analyzed in this study. These Brick types and their material properties were obtained from the material database in WUFI [23].

Table A 1
Hygrothermal properties [26] of the brick types considered in the pre-study.

	Masonry	Extruded	Hand-formed	Historical
Density, ρ (kg/m^3)	1900	1650	1725	1800
Thermal conductivity, λ (W/(m·K))	0.6	0.6	0.6	0.6
Vapor permeability, μ-value (−)	10	9.5	17	15
Water absorption coefficient, A_{cap} (kg/(m^2·min$^{0.5}$))	0.8	3.1	2.3	2.8

Figure A 1 shows the measured and simulated RH at P1 (middle of the brick) and P2 (behind the ACM) for each brick type. The results indicate that the choice of brick had a minor influence on the simulated RH values during the early stage period. However, at later stages, the brick masonry alternative yielded a better agreement between the simulated and measured values in the field. Therefore, brick masonry was selected for the study.

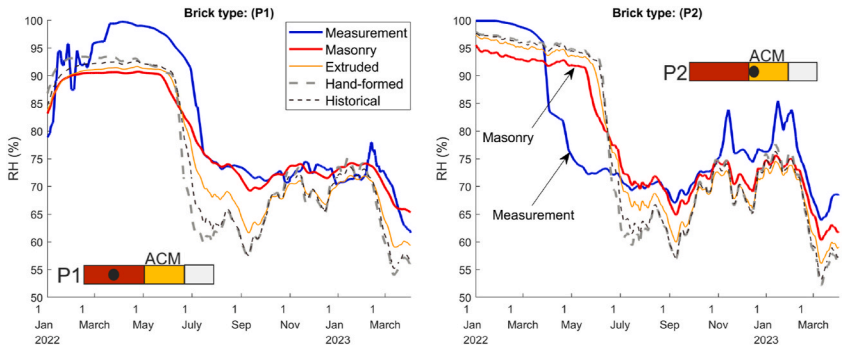

Fig. A 1. Simulated RH using different brick types in the simulations, and the in-field measured RH. Left: In the middle of the brick (P1). Right: Behind the ACM (P2).

Interior climate

Three alternatives were tested in the simulations to account for the unknown interior climate in the field: 1) completely unheated interior that followed the exterior climate, 2) partially heated interior with a temperature profile being five degrees higher than the exterior, 3) fully heated interior based on the standard EN 15026 [31]. For the second alternative, the interior RH was calculated based on the elevated interior temperature and the vapor content in the exterior air; no additional moisture supply was assumed in the interior of the building. The brick masonry was chosen in all three cases.

Figure A 2 shows the measured and simulated RH in positions P1 and P2 for the different interior climates. During the first half of the period, a large discrepancy was observed between all simulations and the measurement results. However, for the rest of the period, the alternative with a heated interior corresponding to five degrees higher temperatures showed a closer match to the measurement results. Therefore, this case was selected for the study.

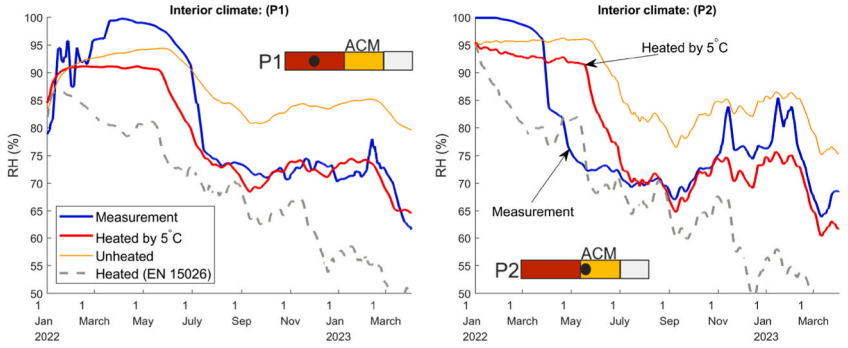

Fig. A 2. Simulated RH using different interior climate conditions in the simulations, and the RH measured in the field. Left: In the middle of the brick (P1). Right: Behind the ACM (P2).

Water absorption coefficient of ACM and outer coating mortar

Previous research [34] has suggested that the A_{cap} of the ACM may increase by five times after exposure to three wetting and drying cycles. The value of A_{cap} directly impacts the calculated liquid water transport coefficients and consequently the moisture transport in the simulations, as expressed in Eq. (1). To evaluate the potential impact of uncertainty in the A_{cap} of the ACM but also the outer mortar, four simulation cases were defined as summarized in Table A 2.

Table A 2. The four cases defined for the sensitivity analyses considering the A_{cap} (kg/(m^2·min$^{0.5}$)) of ACM and outer mortar.

	Description	ACM	Outer coating mortar
Case 1	Measured A_{cap}	0.04	0.08
Case 2	Increased A_{cap} for outer mortar	0.04	0.4
Case 3	Increased A_{cap} for outer mortar and ACM	0.2	0.4
Case 4	Increased A_{cap} for ACM	0.2	0.08

Figure A 3 presents the simulation results for all four cases, showing that changing the A_{cap} of the ACM or outer coating mortar did not improve the agreement with the measurements during the early stage of the period. For the rest of the period, the simulations using the actual measured A_{cap} values (case 1) showed better agreement with the measurements than cases 2–4, where the increased values of A_{cap} were used. Therefore, the actual measured A_{cap} values were selected for the study.

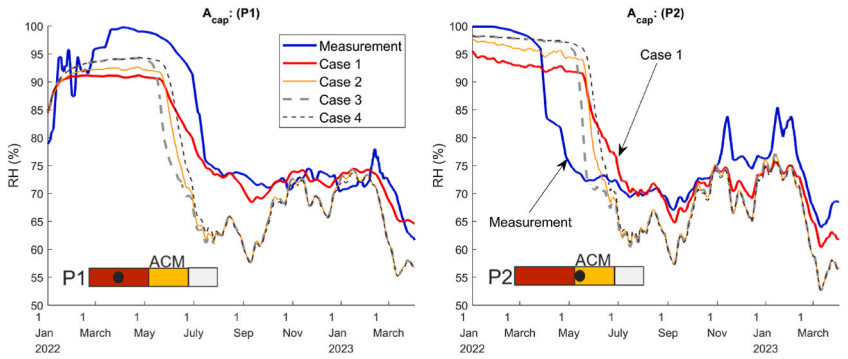

Fig. A 3. In-field and simulated RH for the four defined cases considering different A_{cap} of the ACM and the outer mortar. Left: In the middle of the brick (P1). Right: Behind the ACM (P2).

Appendix B. Simulation case study-scenario 2

Appendix B presents the simulation results for scenario 2, which evaluated the long-term hygrothermal performance of the ACM-system oriented towards the north with the lowest drying potential.

Figure B 1 illustrates the calculated W_{tot} in the test wall with ACM at various locations over five years of simulations. Without rain, Gothenburg showed the highest W_{tot} at steady state (6.6 kg/m^3), 22 % more than Kiruna (5.4 kg/m^3). With rainwater absorption (AFR: 0.7), the maximum W_{tot} in Gothenburg and Kiruna was up to 10.2 kg/m^3 and 10.5 kg/m^3, respectively. The ACM-system demonstrated no moisture accumulation over an extended period.

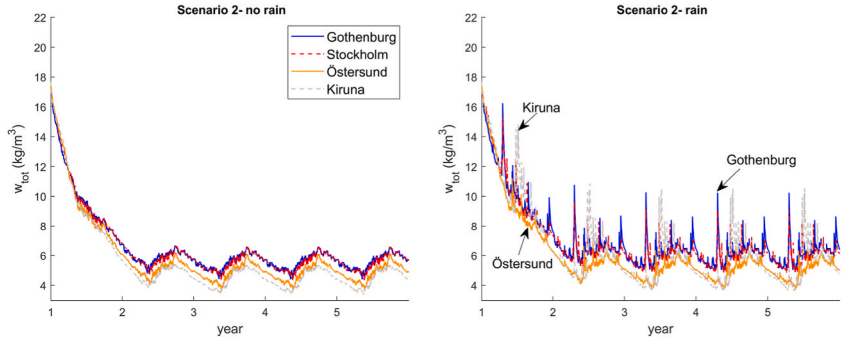

Fig. B 1. Simulated water content in the test wall with ACM as being in four Swedish cities. Left: No rain. Right:- Rain.

Fig. B 2 presents the simulated RH at the interface between the ACM and brick (P2) in the north-oriented test wall for the four Swedish cities studied. Assuming no rainwater absorption (AFR: 0), the RH for Gothenburg and Stockholm ranged between 37 and 63 %, while for Östersund and Kiruna, the values ranged between 25-60 % and 20–56 %, respectively. With rainwater absorption, the highest and lowest RH in P2 were found in Kiruna with 76 % and 22 %, respectively. Stockholm and Gothenburg had comparable RH ranging from 40 to 70 %. For scenario 2, no condensation is expected at the interface between the ACM and the brick.

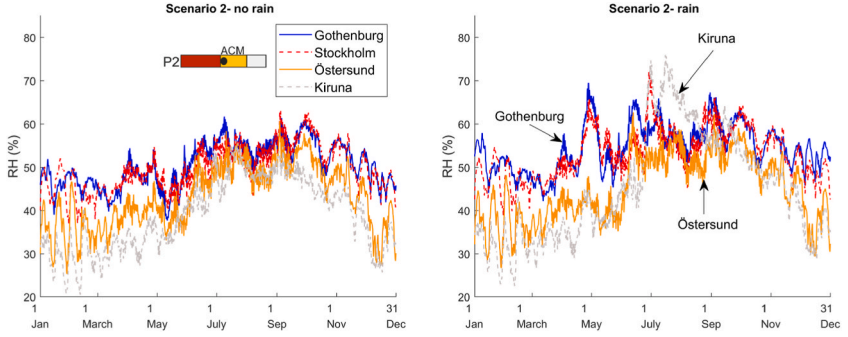

Fig. B 2. Simulated RH at the interface between the ACM and brick (P2), corresponding to the last year of simulations for all four cities. Left: No rain. Right: Rain.

Fig. B 3 depicts the simulated average RH and corresponding thermal conductivity of the ACM layer in the north-oriented test wall for the four Swedish cities. Without rain, the average RH ranged from 41 % (Östersund) to 73 % (Stockholm), with a median in Stockholm (highest) approximately 13 % higher than in Kiruna (lowest). With rain absorption, the RH ranged from 41 % (Östersund) to 85 % (Kiruna), with a median in Stockholm (highest) around 12 % higher than in Kiruna (lowest). As shown in Figure B 3 (c, d), for

the case without rain, the moisture-dependent thermal conductivity of the ACM was between 0.042 and 0.045 W/(m·K). For the case with rain, the thermal conductivity increased to 0.042–0.048 W/(m·K).

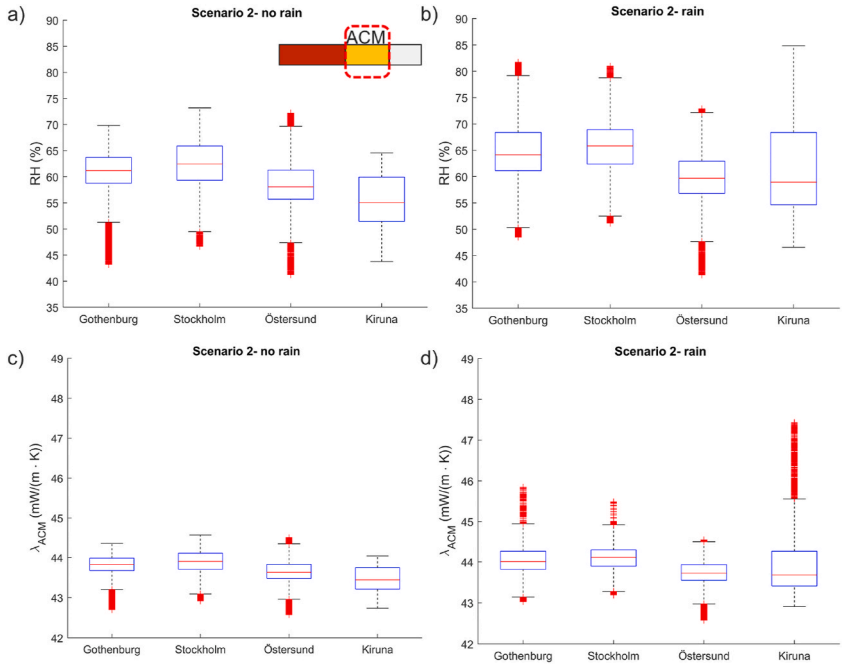

Fig. B 3. a,b: Simulated average RH in the layer of ACM. c,d: Calculated moisture-dependent thermal conductivity of the ACM. Left: No rain. Right: Rain.

References

[1] A.N. Karim, P. Johansson, A. Sasic Kalagasidis, Knowledge gaps regarding the hygrothermal and long-term performance of aerogel-based coating mortars, Construct. Build. Mater. 314 (2022) 125602, https://doi.org/10.1016/J.CONBUILDMAT.2021.125602.

[2] A.N. Karim, Aerogel-based Plasters for Renovation of Buildings in Sweden: Identification of Possibilities, Information Deficiencies and Challenges, Licenciate Thesis, Chalmers University of Technology, 2021.

[3] A.N. Karim, P. Johansson, A. Sasic Kalagasidis, Increasing water absorptivity of an aerogel-based coating mortar in subsequent wetting and drying, Gels 8 (2022) 764, https://doi.org/10.3390/GELS8120764, 2022;8:764.

[4] S. Ximenes, A. Silva, A. Soares, I. Flores-Colen, J. de Brito, Parametric analysis to study the influence of aerogel-based renders' components on thermal and mechanical performance, Materials 9 (2016), https://doi.org/10.3390/ma9050336, 336–255.

[5] T. Stahl, K.G. Wakili, E. Heiduk, Stability relevant properties of an SiO2 aerogel-based rendering and its application on buildings, Sustain. Times 13 (2021) 10035, https://doi.org/10.3390/SU131810035, 2021;13:10035.

[6] M. Ibrahim, E. Wurtz, P.H. Biwole, P. Achard, H. Sallee, Hygrothermal performance of exterior walls covered with aerogel-based insulating rendering, Energy Build. 84 (2014) 241–251, https://doi.org/10.1016/J.ENBUILD.2014.07.039.

[7] M. Ibrahim, P.H. Biwole, P. Achard, E. Wurtz, G. Ansart, Building envelope with a new aerogel-based insulating rendering: experimental and numerical study, cost analysis, and thickness optimization, Appl. Energy 159 (2015) 490–501, https://doi.org/10.1016/J.APENERGY.2015.08.090.

[8] K. Ghazi Wakili, C. Dworatzyk, M. Sanner, A. Sengespeick, M. Paronen, T. Stahl, Energy efficient retrofit of a prefabricated concrete panel building (Plattenbau) in Berlin by applying an aerogel based rendering to its façades, Energy Build. 165 (2018) 293–300, https://doi.org/10.1016/J.ENBUILD.2018.01.050.

[9] M. Pedroso, I. Flores-Colen, J.D. Silvestre, M.G. Gomes, L. Silva, P. Sequeira, et al., Characterisation of a multilayer external wall thermal insulation system. Application in a Mediterranean climate, J. Build. Eng. 30 (2020) 101265, https://doi.org/10.1016/J.JOBE.2020.101265.

[10] M. Ibrahim, L. Bianco, O. Ibrahim, E. Wurtz, Low-emissivity coating coupled with aerogel-based plaster for walls' internal surface application in buildings: energy saving potential based on thermal comfort assessment, J. Build. Eng. (2018), https://doi.org/10.1016/j.jobe.2018.04.008.

[11] M. Pedroso, J.D. Silvestre, I. Flores-Colen, M.G. Gomes, Environmental impact of wall multilayer coating systems containing aerogel-based fibre-enhanced thermal renders, J. Build. Eng. 76 (2023) 107322, https://doi.org/10.1016/j.jobe.2023.107322.

[12] T. Stahl, K. Ghazi Wakili, S. Hartmeier, E. Franov, W. Niederberger, M. Zimmermann, Temperature and moisture evolution beneath an aerogel based rendering applied to a historic building, J. Build. Eng. 12 (2017) 140–146, https://doi.org/10.1016/J.JOBE.2017.05.016.

[13] T. Béjat, D. Therme, Experimental Analysis of the Hygrothermal Performance of New Aerogel-Based Insulating Building Materials in Real Weather Conditions: Full-Scale Application Study, vol. 163, Springer Singapore, 2020, https://doi.org/10.1007/978-981-32-9868-2.

[14] E. Fenoglio, S. Fantucci, M. Perino, V. Serra, M. Dutto, V. Marino, Energy retrofit of residential buildings with a novel super-insulating aerogel-based plaster, AiCARR J 61 (2020) 44–48.

[15] S. Fantucci, E. Fenoglio, V. Serra, Laboratory vs field performance of innovative thermal insulating plasters, in: XV Int. Conf. Durab. Build. Mater. Components (DBMC 2020), CIMNE, 2020, https://doi.org/10.23967/dbmc.2020.178.

[16] S. Fantucci, E. Fenoglio, G. Grosso, V. Serra, M. Perino, V. Marino, et al., Development of an aerogel-based thermal coating for the energy retrofit and the prevention of condensation risk in existing buildings, Sci Technol Built Environ 25 (2019) 1178–1186, https://doi.org/10.1080/23744731.2019.1634931.

[17] K. Ghazi Wakili, T. Stahl, E. Heiduk, M. Schuss, R. Vonbank, U. Pont, et al., High performance aerogel containing plaster for historic buildings with structured façades, Energy Proc. 78 (2015) 949–954, https://doi.org/10.1016/j.egypro.2015.11.027.

[18] M. Schuss, U. Pont, A. Mahdavi, Long-term experimental performance evaluation of aerogel insulation plaster, Energy Proc. 132 (2017) 508–513, https://doi.org/10.1016/J.EGYPRO.2017.09.696.

[19] M. Kottek, J. Grieser, C. Beck, B. Rudolf, F. Rubel, World map of the Köppen-Geiger climate classification updated, Meteorol. Z. 15 (2006) 259–263, https://doi.org/10.1127/0941-2948/2006/0130.
[20] Wall Systems, HECK AERO iP, 2022. https://www.wall-systems.com/produkte/daemmputze-innendaemmung/aero-ip. (Accessed 23 October 2022).
[21] Weber, Webertherm 342 Fasadbruk, 2022. https://www.se.weber/fasad-puts-och-murbruk-produkter-och-system/putsbruk/webertherm-342-fasadbruk. (Accessed 23 October 2022).
[22] Lufft Rain, Gauge WTB100. https://www.lufft.com/products/precipitation-sensors-287/rain-gauge-wtb100-2311/, 2023. (Accessed 25 April 2023).
[23] M. Guizzardi, J. Carmeliet, D. Derome, Risk analysis of biodeterioration of wooden beams embedded in internally insulated masonry walls, Construct. Build. Mater. 99 (2015) 159–168, https://doi.org/10.1016/j.conbuildmat.2015.08.022.
[24] J. Maia, M. Pedroso, N.M.M. Ramos, P.F. Pereira, I. Flores-Colen, M. Glória Gomes, et al., Hygrothermal performance of a new thermal aerogel-based render under distinct climatic conditions, Energy Build. 243 (2021) 111001, https://doi.org/10.1016/j.enbuild.2021.111001.
[25] H.M. Künzel, Simultaneous Heat and Moisture Transport in Building Components : One- and Two-Dimensional Calculation Using Simple Parameters. PhD Thesis, IRB Verlag Stuttgart, 1995.
[26] I.B.P. Fraunhofer, WUFI. https://wufi.de/en/, 2020. (Accessed 15 June 2021). https://wufi.de/en/.
[27] EN 1015-19, Methods of Tests for Mortar for Masonry – Part 19: Determination of Water Vapour Permeability of Hardened Rendering and Plastering Mortars, 1999.
[28] EN 1015-18, Methods of Test for Mortar for Masonry – Part 18: Determination of Water Absorption Coefficient Due to Capillary Action of Hardened Mortar, 2002.
[29] ISO 22007-2. Plastics — Determination of Thermal Conductivity and Thermal Diffusivity — Part 2: Transient Plane Heat Source (Hot Disc) Method, 2015.
[30] A.N. Karim, A.S. Kalagasidis, P. Johansson, Moisture absorption of an aerogel-based coating system under different wetting scenarios, Build. Environ. 245 (2023), https://doi.org/10.1016/j.buildenv.2023.110905.
[31] EN 15026, Hygrothermal Performance of Building Components and Building Elements - Assessment of Moisture Transfer by Numerical Simulation, 2007.
[32] ASHRAE, Standard 160-2016, in: Criteria for Moisture-Control Design Analysis in Buildings, ASHRAE, Atlanta, GA, 2016.
[33] SMHI, Ladda ner meteorologiska observationer. https://www.smhi.se/data/meteorologi/ladda-ner-meteorologiska-observationer#param=precipitationHourlySum,stations=all,stationid=161910, 2021. (Accessed 15 September 2021).
[34] A.N. Karim, P. Johansson, A.S. Kalagasidis, Increasing water absorptivity of an aerogel-based coating mortar in subsequent wetting and drying, Gels 8 (2022) 764, https://doi.org/10.3390/GELS8120764, 2022;8:764.